Optical absorption driven by dynamical symmetry breaking in indium oxide

Andrew J. Morris[1] and Bartomeu Monserrat[2,*]

[1] *School of Metallurgy and Materials, University of Birmingham, Edgbaston, Birmingham B15 2TT, United Kingdom*
[2] *TCM Group, Cavendish Laboratory, University of Cambridge, J. J. Thomson Avenue, Cambridge CB3 0HE, United Kingdom*

(Dated: August 8, 2018)

Indium oxide is a wide band gap semiconductor that provides the platform for most n-type transparent conductors. Optical absorption is dominated by a strong edge starting at the optical gap around 3.7 eV, but the material also exhibits a prominent absorption tail starting around 2.7 eV. We use first principles methods to show that this tail arises from interband transitions that are dipole forbidden at the static lattice level, but become dipole allowed via a dynamical symmetry breaking induced by nuclear motion. We also report the temperature dependence of the absorption onset, which exhibits a red shift with heating, driven by a combination of electron-phonon coupling and thermal expansion. We argue that the role of dynamical symmetry breaking in optical absorption is a general feature of semiconductors and that the computational design of novel materials for optical applications, ranging from transparent conductors to solar cells, should incorporate the lattice dynamics of the crystal.

Indium oxide (In_2O_3) is a versatile wide band gap semiconductor [1] which finds applications in areas ranging from gas sensors [2] to optoelectronic devices such as solar cells or flat panel displays [3–8]. The optoelectronic applications arise mostly due to the use of tin-doped In_2O_3 as an n-type transparent conductor, and a large body of research exists regarding both optical and transport properties of this material.

It might therefore appear surprising that even basic quantities such as the nature of the band gap of In_2O_3 continue to attract intensive research efforts [9–18]. Early experimental reports suggested that In_2O_3 had a direct band gap around 3.7 eV exhibiting strong optical absorption, and an indirect band gap around 2.7 eV exhibiting much weaker absorption [9, 11]. However, first principles calculations invariably reported either direct band gaps or slightly indirect band gaps of maximum size 0.05 eV [12, 13]. Walsh and co-workers resolved this conundrum by a combination of group theory arguments, first principles calculations, and x-ray spectroscopy, arguing that the absorption tail observed below the optical gap at 3.7 eV arises from weak transitions that are formally forbidden due to dipole selection rules [14]. Similar phenomena have been reported in other systems [19, 20]. Although the dipole-forbidden picture of the band gap of In_2O_3 is now largely accepted, available first principles calculations underestimate the strength of the measured absorption tail by multiple orders of magnitude [17] thus severely limiting their predictive power.

In this work, we resolve this discrepancy showing that the absorption tail in In_2O_3 arises from a dynamical symmetry breaking that allows weak optical absorption across formally dipole forbidden states. We accomplish this by performing first principles optical absorption calculations that include the effects of lattice dynamics [21, 22], thus extending the applicability of computational techniques used to explain absorption in indirect band gap semiconductors [23–28] and absorption by free carriers in doped semiconductors [29–31].

Apart from providing a microscopic picture for the optical absorption of In_2O_3, we expect that the methodology used in this work will prove useful in the exploration of novel materials for transparent conducting applications. This line of research is motivated by the scarcity of indium and the associated need for replacement n-type transparent conductors, as well as the need for a good p-type transparent conductor. Alternatives range from using other transparent conducting oxides such as $BaSnO_3$ [32–35], to novel design principles that include non-oxide semiconductors [36, 37], graphene [38], metal nanowires [39], correlated metals [40], or bulk metals engineered to have low interband absorption [41]. The optical properties of these materials typically exhibit indirect transitions or rely on the enforcement of selection rules to ensure transparency in the optical range [27, 28, 37, 41]. A full understanding of the optical properties of these candidate transparent conductors thus requires the inclusion of lattice dynamics as described in this work.

We consider the ground state cubic $Ia\bar{3}$ structure of In_2O_3 with 40 atoms in the primitive cell. We perform first principles calculations based on density-functional theory (DFT) [42, 43] as implemented in the CASTEP [44] plane wave pseudopotential code. Our DFT calculations use the Perdew-Burke-Ernzerhof (PBE) generalised gradient approximation to the exchange-correlation functional [45], which is known to underestimate band gap sizes and therefore we correct this by using a scissor operator [46, 47] of +2.116 eV, chosen so that the static lattice optical band gap corresponds to an energy of 3.75 eV, consistent with experimental reports [9, 10, 15]. Note that the absorption tail starts at lower energies of about 2.7 eV. We additionally perform lattice dynamics

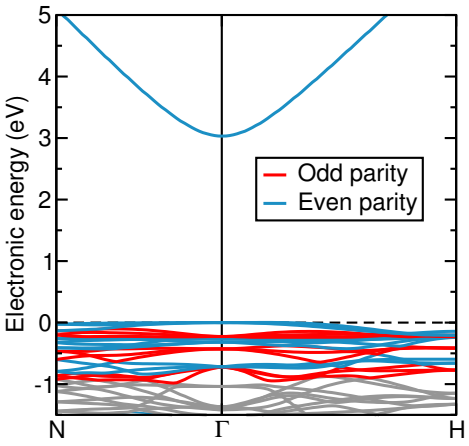

FIG. 1. Band structure of cubic In_2O_3. The CBM and the top 18 valence bands are labelled according to the even (blue) or odd (red) parity of the corresponding states at the Γ point.

calculations based on the finite displacement method [48] with nondiagonal supercells [49] and use these within the Williams-Lax theory [21, 22, 24, 25] to calculate optical absorption at finite temperature. The optical constants are calculated using the OPTADOS package [50, 51]. Further details of the calculations are described in the Supplemental Material [52].

In the single-electron band theory of solids optical absorption can be studied by considering transitions between electronic levels induced by a time-dependent electromagnetic field of amplitude A_0 and polarisation $\hat{\mathbf{e}}$. We consider an initial electronic state $|\psi_{v\mathbf{k}}\rangle$ of energy $\epsilon_{v\mathbf{k}}$ with valence band index v and momentum $\mathbf{k}$ and a conduction band final state $|\psi_{c\mathbf{k}}\rangle$ of energy $\epsilon_{c\mathbf{k}}$. The first order transition probability between these two states is given by Fermi's golden rule within the dipole approximation:

$$\mathcal{P}_{v\mathbf{k}\to c\mathbf{k}} = \frac{2\pi}{\hbar}\left(\frac{eA_0}{m\gamma}\right)^2 |M_{cv\mathbf{k}}|^2 \delta(\epsilon_{c\mathbf{k}} - \epsilon_{v\mathbf{k}} - \hbar\omega), \quad (1)$$

where we have denoted the speed of light, γ, (to avoid confusion with conduction states), m is the electron mass, e the electron charge, $\hbar\omega$ is the energy of the absorbed photon, and the optical matrix element is

$$M_{cv\mathbf{k}} = \langle\psi_{c\mathbf{k}}|\hat{\mathbf{e}}\cdot\mathbf{p}|\psi_{v\mathbf{k}}\rangle. \quad (2)$$

Selection rules arising from symmetry are an important feature of the optical matrix element of Eq. (2). The electric dipole operator $\mathbf{p}$ has odd symmetry under inversion, which implies that $M_{cv\mathbf{k}} = 0$ for transitions between states of the same parity. These states can arise in systems with inversion symmetry C_i, whose two one-dimensional irreducible representations are labelled by their even (+1) and odd (−1) parities.

Cubic In_2O_3 is a centrosymmetric crystal, and the electron states at the Γ point can be classified according to their parity eigenvalues because the symmetry of $\mathbf{k} = 0$ is the full point group symmetry of the crystal and therefore includes inversion (see Fig. 1 and Table I). Walsh and co-workers [14] showed that the minimum direct band gap of In_2O_3, which occurs at the Γ point as shown in Fig. 1, is dipole forbidden because the valence band maximum (VBM) and the conduction band minimum (CBM) are both of even parity. They further demonstrated that strong optical absorption only occurs from the valence band at −0.725 eV (see Table I) which is of odd parity and therefore dipole allowed. Although there are two sets of valence bands at higher energies of −0.227 eV and −0.428 eV which are also dipole allowed, their optical matrix elements are small (see Table I), and therefore strong optical absorption only occurs from the −0.725 eV valence band, which determines the so-called optical gap observed in experiments in the range 3.5–3.8 eV [9, 10, 15]. This can be seen in the static lattice absorption spectrum of In_2O_3 shown in Fig. 2, which exhibits a sharp increase at energies around 3.75 eV, the location of the optical gap.

The parity argument provides a convincing explanation for the observation of the optical gap at an energy about 0.7 eV higher than the nominal minimum band gap at 3.03 eV. The weak but dipole allowed transitions from the valence bands at −0.227 eV and −0.428 eV provide an absorption tail at the static lattice level, as shown in Fig. 2. This tail also has contributions from weak absorption arising from states at $\mathbf{k} \neq 0$, for which parity is not a good quantum number and therefore the corresponding optical matrix elements are dipole allowed. The contributions from states at $\mathbf{k} \neq 0$ is weak because for sufficiently small $\mathbf{k}$ the states are largely aligned with their $\mathbf{k} = 0$ counterparts, thus exhibiting strongly suppressed optical matrix elements between the VBM and CBM.

However, these weak sub-optical gap contributions are insufficient to account for the experimentally observed tail. First, optical absorption starts at energies in the range 2.6–2.9 eV [9, 10, 15, 17] but the tail exhibited by the calculated static lattice absorption coefficient in Fig. 2 starts above 3 eV. Second, the calculated absorption coefficient at the tail is multiple orders of magnitude too weak compared to experiment [17]. For example, the experimental absorption coefficient is about 500 cm^{-1} at 2.9 eV, and reaches 1500 cm^{-1} at 3.0 eV [17], values which are two to three orders of magnitude higher than those of static lattice calculations (see Fig. 2 and Ref. [14]). We note that our static lattice absorption coefficient results agree with those of Ref. [14], but disagree with those recently reported in Ref. [55], in which a significant overestimation of the absorption coefficient compared to experiment is calculated.

Lattice dynamics provides an explanation for the stronger tail observed experimentally. Within the adiabatic approximation, electronic quantities can be modi-

TABLE I. Electronic and optical properties of In_2O_3 at the BZ center. Band energies are measured with respect to the valence band maximum, and we report the band degeneracies, parities (determined using C2X [53]), and the optical matrix elements $|M_{cv\Gamma}|^2 = |\langle\psi_{c\Gamma}|\hat{\mathbf{e}}\cdot\mathbf{p}|\psi_{v\Gamma}\rangle|^2$ between the CBM at 3.032 eV and a number of valence band states. Results are shown at the static lattice level, and for thermal line distortions [54] corresponding to 0 K (zero-point motion) and 300 K. For bands that are degenerate at the static lattice level, we consider the average over the optical matrix elements at 0 K and 300 K.

Band energy (eV)	Degeneracy	Parity	$\lvert M_{cv\Gamma}\rvert^2$ (static)	$\lvert M_{cv\Gamma}\rvert^2$ (0 K)	$\lvert M_{cv\Gamma}\rvert^2$ (300 K)
3.032	1	1	–	–	–
0.000	3	1	0.000	0.006	0.010
−0.227	3	−1	0.015	0.020	0.023
−0.238	1	1	0.000	0.025	0.033
−0.264	2	1	0.000	0.002	0.007
−0.317	3	1	0.000	0.020	0.039
−0.428	3	−1	0.008	0.044	0.052
−0.719	3	1	0.000	0.346	0.320
−0.725	3	−1	0.800	0.346	0.320

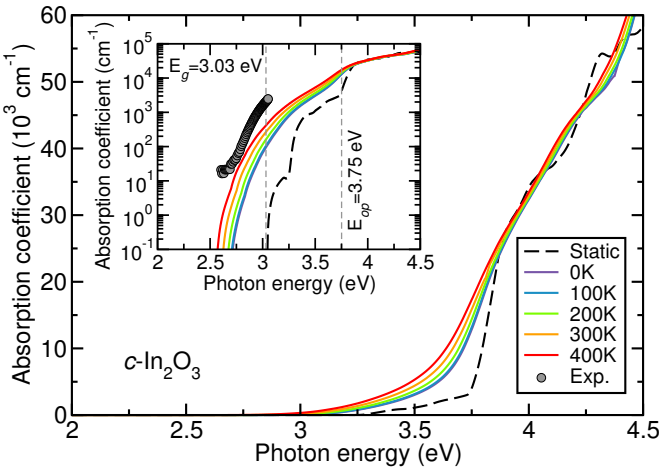

FIG. 2. Absorption coefficient of In_2O_3 at the static lattice level of theory (dashed black line), and including lattice dynamics at multiple temperatures (solid lines). The inset shows the same data around the absorption onset, with dashed grey vertical lines depicting the location of the minimum band gap E_g and the optical band gap E_{op}. The inset also shows a comparison with the experimental data (circles) reported in Ref. [17].

fied by nuclear motion by considering the average over all nuclear configurations distributed according to the temperature dependent nuclear density [56]. Consider a generic atomic configuration $\mathbf{u} = \{u_{\nu\mathbf{q}}\}$ where $u_{\nu\mathbf{q}}$ is the amplitude of the normal mode of vibration labelled by phonon branch ν and wave vector $\mathbf{q}$. In this notation, the static lattice corresponds to $\mathbf{u} = \mathbf{0}$. The optical matrix element becomes

$$M_{cv\mathbf{k}}(\mathbf{u}) = \langle\psi_{c\mathbf{k}}(\mathbf{u})|\hat{\mathbf{e}}\cdot\mathbf{p}|\psi_{v\mathbf{k}}(\mathbf{u})\rangle. \quad (3)$$

Most nuclear configurations $\mathbf{u}$ break inversion symmetry, and therefore parity is no longer a good quantum number, even for the states at $\mathbf{k} = 0$. It follows that the optical matrix elements at Γ that are dipole forbidden at the static lattice level become dipole allowed when lattice dynamics are incorporated. This *dynamical symmetry breaking* leads to enhanced absorption compared to the static lattice absorption. This is shown in Fig. 2, where we plot the optical absorption coefficient including lattice dynamics at 0 K (quantum zero-point motion) as well as finite temperatures up to 400 K. The vibrationally averaged absorption onset undergoes a red shift to about 2.6 eV, recovering good agreement with experimental observations. Furthermore the absorption coefficient increases by multiple orders of magnitude for photon energies below the optical gap, reaching a value between 100 and 1000 cm^{-1} between 2.9 and 3.1 eV. These values compare favourably with experiment [17], allowing for an uncertainty of up to 0.2 eV in the scissor operator that we have chosen to fix the static lattice optical band gap at 3.75 eV. We emphasise that our approach allows us to include absorption tails and the shift of absorption peaks with temperature on the same footing.

To quantify the effects of dynamical symmetry breaking on the dipole-forbidden optical matrix elements, we compare the optical matrix elements at the static lattice level with those including nuclear dynamics in Table I. The dynamical matrix elements at 0 K and 300 K are calculated from atomic configurations corresponding to points on thermal lines at those temperatures [54]. These are mean configurations of the system for which the value of an electronic quantity (such as the optical matrix element) is equal to the vibrational average of that quantity as a consequence of the mean-value theorem for integrals [54, 56]. The results in Table I show that the matrix elements involving valence states of even parity vanish at the static lattice level due to the dipole selection rules.

However, the corresponding matrix elements at 0 K and 300 K are non-zero, and their magnitude increases with increasing temperature, driven by the dynamical symmetry breaking induced by lattice vibrations. We can also see that optical transitions from states at −0.227 eV and −0.428 eV, which are not dipole forbidden but have small matrix elements at the static lattice level, also increase in magnitude with increasing temperature. The states at −0.719 eV are even and therefore transitions from them are dipole forbidden, and the states at −0.725 eV are odd and transitions are dipole allowed, with the latter exhibiting large matrix elements associated with the optical gap of In_2O_3. When lattice dynamics are included, these two sets of bands, which are very close in energy at the static lattice level, become mixed at the dynamical level, and we therefore report the average over all six bands in Table I. Inspecting individual matrix elements shows that their magnitudes are similar to the reported average, suggesting that the dynamics makes these two sets of bands equivalent.

We note that additional contributions to transitions between formally dipole forbidden states arise from second order perturbation theory [57]. These transitions bypass the selection rules because they are mediated by an intermediate state i that could be of a different parity to the initial and final states. We expect these contributions to be small because the transition strength is proportional to $(\epsilon_{i\mathbf{k}} - \epsilon_{v\mathbf{k}} \mp \hbar\omega)^{-1}$, and the highly dispersive conduction band of In_2O_3 leads to an isolated conduction band minimum and thus to a large denominator in the second order perturbative term which suppresses its value. Another contribution would arise from the presence of defects, which statically break inversion symmetry and could therefore also allow optical transitions between the band edges at the Γ point that would contribute to the absorption tails. We finally note that excitonic contributions have been reported for In_2O_3 [18], but the symmetry arguments provided in this work are independent of those.

In the Supplemental Material [52] we report analogous optical absorption calculations including the effects of lattice dynamics for two additional polymorphs of In_2O_3 which have also been stabilised under ambient conditions [58–65], finding similar results to those reported here for the cubic ground state structure.

The phonon-assisted optical absorption reported so far has been calculated at the fixed equilibrium volume. The equilibrium lattice parameter of cubic In_2O_3 calculated using PBE is 10.293 Å, a value that overestimates the experimental lattice parameter by about 2% [66], a typical number for PBE-based volumes. However, here we are interested in thermal expansion, for which PBE reproduces the correct trend.

Using the quasiharmonic approximation [67], we consider In_2O_3 structures with lattice parameters ranging from 10.293 Å to 10.367 Å in steps of 0.011 Å, and relaxed internal coordinates. For each of these structures we calculate the Helmholtz free energy using the harmonic approximation to lattice dynamics. The diagram on the left of Fig. 3 shows the calculated Helmholtz free energy relative to the static lattice energy of In_2O_3 as a function of lattice parameter and for temperatures ranging from 0 K to 400 K. The black triangles indicate the minimum of each temperature curve, and provide the quasiharmonic estimate of the equilibrium volume at that temperature. Available experimental data of thermal expansion in In_2O_3 only starts at 273.15 K, showing an increase of the cubic lattice parameter from 300 K to 400 K of 0.06% by the dilatometric method [68] and of 0.09% by the more accurate x-ray method [66]. The calculated change of 0.12% between 300 K and 400 K is closer to the x-ray results, but overestimates the lattice expansion by an amount similar to the discrepancy between the two experimental methods.

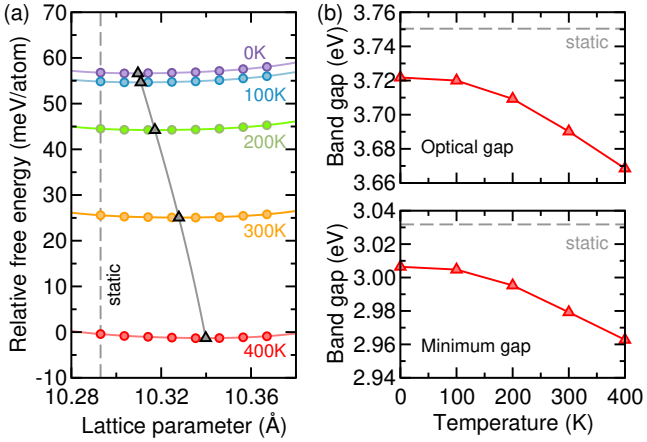

FIG. 3. Thermal expansion of In_2O_3. (a) Relative Helmholtz free energy as a function of the cubic lattice parameter for a range of temperatures. The black triangles indicate the minima of the corresponding Helmholtz free energy curves. (b) Temperature dependence of the optical (top) and minimum (bottom) band gaps of In_2O_3 arising from thermal expansion.

The diagram on the right of Fig. 3 shows the temperature dependence of the optical and minimum band gaps of In_2O_3 arising from the effects of thermal expansion. The optical band gap at 0 K (including quantum zero-point motion) is 28 meV lower in energy than the static lattice band gap of 3.750 eV. Increasing temperature to 400 K leads to a further decrease in the size of the band gap of 53 meV from 0 K. The minimum band gap exhibits a weaker temperature dependence, with a decrease of 25 meV due to quantum zero-point motion from a static lattice value of 3.032 eV, and a further decrease of 44 meV to 400 K.

Comparing the change in the band gap arising from thermal expansion in Fig. 3 to the change arising from the electron-phonon interaction in Fig. 2 we observe that the electron-phonon coupling contribution dominates. For

example, the absorption onset decreases by 140 meV due to electron-phonon coupling when temperature increases from 0 K to 400 K, whereas the corresponding decrease arising from thermal expansion is 44 meV. Adding these two contributions leads to an overall red shift of the band gap of 184 meV, which corresponds to 60% of the 316 meV red shift reported experimentally [17]. Recent calculations have demonstrated that semilocal DFT tends to underestimate the strength of electron-phonon coupling in both metals [69–71] and semiconductors [72, 73], and we therefore attribute the discrepancy between our calculations and the experimental temperature dependence to the use of semilocal DFT in our study.

In summary, we have studied optical absorption in In_2O_3 polymorphs showing that, although the minimum band gap corresponds to a dipole forbidden optical transition, this transition becomes allowed when nuclear vibrations dynamically break the inversion symmetry of the system. Using first principles calculations, we predict an absorption coefficient for the absorption tail of cubic In_2O_3 that is in good agreement with experimental observations, thereby resolving a longstanding disagreement between theory and experiment of multiple orders of magnitude in the optical absorption coefficient. Our calculations also show a significant red shift of the absorption onset with increasing temperature, with contributions from both electron-phonon coupling and thermal expansion.

More generally, our results demonstrate that formally forbidden transitions in semiconductors can become allowed driven by dynamical symmetry breaking. This has important consequences to understand the optical properties of known semiconductors such as In_2O_3, and also for the computational design of novel materials for applications ranging from transparent conductors to solar cells.

The authors would like to acknowledge R. J. Nicholls for helpful discussions. B.M. acknowledges support from the Winton Programme for the Physics of Sustainability, and from Robinson College, Cambridge, and the Cambridge Philosophical Society for a Henslow Research Fellowship. Data used in this work are available via the Cambridge Data Repository at [insert DOI].

* bm418@cam.ac.uk

[1] Oliver Bierwagen, "Indium oxide – a transparent, wide-band gap semiconductor for (opto)electronic applications," Semicond. Sci. Technol. **30**, 024001 (2015).

[2] Martin Liess and Harald Steffes, "The modulation of thermoelectric power by chemisorption: A new detection principle for microchip chemical sensors," J. Electrochem. Soc. **147**, 3151–3153 (2000).

[3] I. Hamberg and C. G. Granqvist, "Evaporated Sn-doped In_2O_3 films: Basic optical properties and applications to energy-efficient windows," J. Appl. Phys. **60**, R123–R160 (1986).

[4] GeeSung Chae, "A modified transparent conducting oxide for flat panel displays only," Jpn. J. Appl. Phys. **40**, 1282 (2001).

[5] C.G. Granqvist and A. Hultker, "Transparent and conducting ITO films: new developments and applications," Thin Solid Films **411**, 1–5 (2002).

[6] A. N. Tiwari, G. Khrypunov, F. Kurdzesau, D. L. Btzner, A. Romeo, and H. Zogg, "CdTe solar cell in a novel configuration," Prog. Photovolt. Res. Appl. **12**, 33–38 (2004).

[7] A. Porch, D. V. Morgan, R. M. Perks, M. O. Jones, and P. P. Edwards, "Transparent current spreading layers for optoelectronic devices," J. Appl. Phys. **96**, 4211–4218 (2004).

[8] Matthew T. Hardy, Casey O. Holder, Daniel F. Feezell, Shuji Nakamura, James S. Speck, Daniel A. Cohen, and Steven P. DenBaars, "Indium-tin-oxide clad blue and true green semipolar InGaN/GaN laser diodes," Appl. Phys. Lett. **103**, 081103 (2013).

[9] R. L. Weiher and R. P. Ley, "Optical properties of indium oxide," J. Appl. Phys. **37**, 299–302 (1966).

[10] C. A. Pan and T. P. Ma, "High-quality transparent conductive indium oxide films prepared by thermal evaporation," Appl. Phys. Lett. **37**, 163–165 (1980).

[11] V. Christou, M. Etchells, O. Renault, P. J. Dobson, O. V. Salata, G. Beamson, and R. G. Egdell, "High resolution x-ray photoemission study of plasma oxidation of indium-tin-oxide thin film surfaces," J. Appl. Phys. **88**, 5180–5187 (2000).

[12] Paul Erhart, Andreas Klein, Russell G. Egdell, and Karsten Albe, "Band structure of indium oxide: Indirect versus direct band gap," Phys. Rev. B **75**, 153205 (2007).

[13] F. Fuchs and F. Bechstedt, "Indium-oxide polymorphs from first principles: Quasiparticle electronic states," Phys. Rev. B **77**, 155107 (2008).

[14] Aron Walsh, Juarez L. F. Da Silva, Su-Huai Wei, C. Körber, A. Klein, L. F. J. Piper, Alex DeMasi, Kevin E. Smith, G. Panaccione, P. Torelli, D. J. Payne, A. Bourlange, and R. G. Egdell, "Nature of the band gap of In_2O_3 revealed by first-principles calculations and X-ray spectroscopy," Phys. Rev. Lett. **100**, 167402 (2008).

[15] P. D. C. King, T. D. Veal, F. Fuchs, Ch. Y. Wang, D. J. Payne, A. Bourlange, H. Zhang, G. R. Bell, V. Cimalla, O. Ambacher, R. G. Egdell, F. Bechstedt, and C. F. McConville, "Band gap, electronic structure, and surface electron accumulation of cubic and rhombohedral In_2O_3," Phys. Rev. B **79**, 205211 (2009).

[16] V. Scherer, C. Janowitz, A. Krapf, H. Dwelk, D. Braun, and R. Manzke, "Transport and angular resolved photoemission measurements of the electronic properties of In_2O_3 bulk single crystals," Appl. Phys. Lett. **100**, 212108 (2012).

[17] K. Irmscher, M. Naumann, M. Pietsch, Z. Galazka, R. Uecker, T. Schulz, R. Schewski, M. Albrecht, and R. Fornari, "On the nature and temperature dependence of the fundamental band gap of In_2O_3," Phys. Status Solidi A **211**, 54–58 (2014).

[18] Joel B. Varley and André Schleife, "Bethe-Salpeter calculation of optical-absorption spectra of In_2O_3 and Ga_2O_3," Semicond. Sci. Technol. **30**, 024010 (2015).

[19] Shunsuke Nozawa, Toshiaki Iwazumi, and Hitoshi Osawa, "Direct observation of the quantum fluctuation controlled by ultraviolet irradiation in $SrTiO_3$," Phys. Rev. B **72**, 121101 (2005).

[20] D. Manuel, D. Cabaret, Ch. Brouder, Ph. Sainctavit, A. Bordage, and N. Trcera, "Experimental evidence of thermal fluctuations on the x-ray absorption near-edge structure at the aluminum K edge," Phys. Rev. B **85**, 224108 (2012).

[21] Ferd E. Williams, "Theoretical low temperature spectra of the thallium activated potassium chloride phosphor," Phys. Rev. **82**, 281–282 (1951).

[22] Melvin Lax, "The Franck-Condon principle and its application to crystals," J. Chem. Phys. **20**, 1752–1760 (1952).

[23] Jesse Noffsinger, Emmanouil Kioupakis, Chris G. Van de Walle, Steven G. Louie, and Marvin L. Cohen, "Phonon-assisted optical absorption in silicon from first principles," Phys. Rev. Lett. **108**, 167402 (2012).

[24] Christopher E. Patrick and Feliciano Giustino, "Unified theory of electron-phonon renormalization and phonon-assisted optical absorption," J. Phys. Condens. Matter **26**, 365503 (2014).

[25] Marios Zacharias, Christopher E. Patrick, and Feliciano Giustino, "Stochastic approach to phonon-assisted optical absorption," Phys. Rev. Lett. **115**, 177401 (2015).

[26] Marios Zacharias and Feliciano Giustino, "One-shot calculation of temperature-dependent optical spectra and phonon-induced band-gap renormalization," Phys. Rev. B **94**, 075125 (2016).

[27] Youngho Kang, Hartwin Peelaers, Karthik Krishnaswamy, and Chris G. Van de Walle, "First-principles study of direct and indirect optical absorption in $BaSnO_3$," Appl. Phys. Lett. **112**, 062106 (2018).

[28] Bartomeu Monserrat, Cyrus E. Dreyer, and Karin M. Rabe, "Phonon-assisted optical absorption in $BaSnO_3$ from first principles," Phys. Rev. B **97**, 104310 (2018).

[29] Emmanouil Kioupakis, Patrick Rinke, André Schleife, Friedhelm Bechstedt, and Chris G. Van de Walle, "Free-carrier absorption in nitrides from first principles," Phys. Rev. B **81**, 241201 (2010).

[30] H. Peelaers, E. Kioupakis, and C. G. Van de Walle, "Free-carrier absorption in transparent conducting oxides: Phonon and impurity scattering in SnO_2," Phys. Rev. B **92**, 235201 (2015).

[31] H. Peelaers, E. Kioupakis, and C. G. Van de Walle, "Fundamental limits on optical transparency of transparent conducting oxides: Free-carrier absorption in SnO_2," Appl. Phys. Lett. **100**, 011914 (2012).

[32] X. Luo, Y. S. Oh, A. Sirenko, P. Gao, T. A. Tyson, K. Char, and S.-W. Cheong, "High carrier mobility in transparent $Ba_{1-x}La_xSnO_3$ crystals with a wide band gap," Appl. Phys. Lett. **100**, 172112 (2012).

[33] Hyung Joon Kim, Useong Kim, Hoon Min Kim, Tai Hoon Kim, Hyo Sik Mun, Byung-Gu Jeon, Kwang Taek Hong, Woong-Jhae Lee, Chanjong Ju, Kee Hoon Kim, and Kookrin Char, "High mobility in a stable transparent perovskite oxide," Appl. Phys. Exp. **5**, 061102 (2012).

[34] Hyung Joon Kim, Useong Kim, Tai Hoon Kim, Jiyeon Kim, Hoon Min Kim, Byung-Gu Jeon, Woong-Jhae Lee, Hyo Sik Mun, Kwang Taek Hong, Jaejun Yu, Kookrin Char, and Kee Hoon Kim, "Physical properties of transparent perovskite oxides (Ba,La)SnO_3 with high electrical mobility at room temperature," Phys. Rev. B **86**, 165205 (2012).

[35] David O. Scanlon, "Defect engineering of $BaSnO_3$ for high-performance transparent conducting oxide applications," Phys. Rev. B **87**, 161201 (2013).

[36] Feng Yan, Xiuwen Zhang, Yonggang G. Yu, Liping Yu, Arpun Nagaraja, Thomas O. Mason, and Alex Zunger, "Design and discovery of a novel half-Heusler transparent hole conductor made of all-metallic heavy elements," Nat. Commun. **6**, 7308 (2015).

[37] Joel B. Varley, Anna Miglio, Viet-Anh Ha, Michiel J. van Setten, Gian-Marco Rignanese, and Geoffroy Hautier, "High-throughput design of non-oxide p-type transparent conducting materials: Data mining, search strategy, and identification of boron phosphide," Chemistry of Materials **29**, 2568–2573 (2017).

[38] F. Bonaccorso, Z. Sun, T. Hasan, and A. C. Ferrari, "Graphene photonics and optoelectronics," Nat. Photon. **4**, 611 (2010).

[39] Jung Yong Lee, Stephen T. Connor, Yi Cui, and Peter Peumans, "Solution-processed metal nanowire mesh transparent electrodes," Nano Lett. **8**, 689–692 (2008).

[40] Lei Zhang, Yuanjun Zhou, Lu Guo, Weiwei Zhao, Anna Barnes, Hai-Tian Zhang, Craig Eaton, Yuanxia Zheng, Matthew Brahlek, Hamna F. Haneef, Nikolas J. Podraza, Moses H. W. Chan, Venkatraman Gopalan, Karin M. Rabe, and Roman Engel-Herbert, "Correlated metals as transparent conductors," Nat. Mater. **15**, 204 (2016).

[41] Xiuwen Zhang, Lijun Zhang, John D. Perkins, and Alex Zunger, "Intrinsic transparent conductors without doping," Phys. Rev. Lett. **115**, 176602 (2015).

[42] P. Hohenberg and W. Kohn, "Inhomogeneous electron gas," Phys. Rev. **136**, B864–B871 (1964).

[43] W. Kohn and L. J. Sham, "Self-consistent equations including exchange and correlation effects," Phys. Rev. **140**, A1133–A1138 (1965).

[44] Stewart J. Clark, Matthew D. Segall, Chris J. Pickard, Phil J. Hasnip, Matt I. J. Probert, Keith Refson, and Mike C. Payne, "First principles methods using CASTEP," Z. Kristallogr. **220**, 567 (2005).

[45] John P. Perdew, Kieron Burke, and Matthias Ernzerhof, "Generalized gradient approximation made simple," Phys. Rev. Lett. **77**, 3865 (1996).

[46] F. Gygi and A. Baldereschi, "Quasiparticle energies in semiconductors: Self-energy correction to the local-density approximation," Phys. Rev. Lett. **62**, 2160–2163 (1989).

[47] Zachary H. Levine and Douglas C. Allan, "Linear optical response in silicon and germanium including self-energy effects," Phys. Rev. Lett. **63**, 1719–1722 (1989).

[48] K. Kunc and Richard M. Martin, "*Ab Initio* force constants of GaAs: A new approach to calculation of phonons and dielectric properties," Phys. Rev. Lett. **48**, 406–409 (1982).

[49] Jonathan H. Lloyd-Williams and Bartomeu Monserrat, "Lattice dynamics and electron-phonon coupling calculations using nondiagonal supercells," Phys. Rev. B **92**, 184301 (2015).

[50] Andrew J. Morris, Rebecca J. Nicholls, Chris J. Pickard, and Jonathan R. Yates, "OptaDOS: A tool for obtaining density of states, core-level and optical spectra from electronic structure codes," Comput. Phys. Commun. **185**, 1477–1485 (2014).

[51] R. J. Nicholls, A. J. Morris, C. J. Pickard, and J. R. Yates, "OptaDOS - a new tool for EELS calculations," J. Phys. Conf. Ser. **371**, 012062 (2012).

[52] See Supplemental Material for numerical details of the first principles calculations, and results for the rhombohedral and orthorhombic polymorphs of In_2O_3.

[53] M.J. Rutter, "C2x: A tool for visualisation and input preparation for Castep and other electronic structure codes," Comput. Phys. Commun. **225**, 174 – 179 (2018).

[54] Bartomeu Monserrat, "Vibrational averages along thermal lines," Phys. Rev. B **93**, 014302 (2016).

[55] J. J. Meléndez and M. Wierzbowska, "In_2O_3 doped with hydrogen: Electronic structure and optical properties from the pseudopotential self-interaction corrected density functional theory and the random phase approximation," J. Phys. Chem. C **120**, 4007–4015 (2016).

[56] Bartomeu Monserrat, "Electron-phonon coupling from finite differences," J. Phys. Condens. Matter **30**, 083001 (2018).

[57] F. Bassani and G. Pastori Parravicini, *Electronic States and Optical Transitions in Solids* (Pergamon Press, 1975).

[58] A. N. Christensen, N. C. Broch, O. von Heidenstam, and A. Nilsson, "Hydrothermal investigation of the systems In_2O_3-H_2O-Na_2O and In_2O_3-D_2O-Na_2O. the crystal structure of rhombohedral In_2O_3 and of $In(OH)_3$," Acta Chem. Scand. **21**, 1046 (1967).

[59] Charles T. Prewitt, Robert D. Shannon, Donald Burl Rogers, and Arthur W. Sleight, "C rare earth oxide-corundum transition and crystal chemistry of oxides having the corundum structure," Inorg. Chem. **8**, 1985–1993 (1969).

[60] T. Atou, K. Kusaba, K. Fukuoka, M. Kikuchi, and Y. Syono, "Shock-induced phase transition of M_2O_3 (M = Sc, Y, Sm, Gd, and In)-type compounds," J. Solid State Chem. **89**, 378–384 (1990).

[61] Ch. Y. Wang, V. Cimalla, H. Romanus, Th. Kups, G. Ecke, Th. Stauden, M. Ali, V. Lebedev, J. Pezoldt, and O. Ambacher, "Phase selective growth and properties of rhombohedral and cubic indium oxide," Appl. Phys. Lett. **89**, 011904 (2006).

[62] M. Sorescu, L. Diamandescu, D. Tarabasanu-Mihaila, and V. S. Teodorescu, "Nanocrystalline rhombohedral In_2O_3 synthesized by hydrothermal and postannealing pathways," J. Mater. Sci. **39**, 675–677 (2004).

[63] S. Zh. Karazhanov, P. Ravindran, P. Vajeeston, A. Ulyashin, T. G. Finstad, and H. Fjellvåg, "Phase stability, electronic structure, and optical properties of indium oxide polytypes," Phys. Rev. B **76**, 075129 (2007).

[64] Maged F. Bekheet, Marcus R. Schwarz, Stefan Lauterbach, HansJoachim Kleebe, Peter Kroll, Ralf Riedel, and Aleksander Gurlo, "Orthorhombic In_2O_3: A metastable polymorph of indium sesquioxide," Angew. Chem. Int. Ed. **52**, 6531–6535 (2013).

[65] Aron Walsh and David O. Scanlon, "Polymorphism of indium oxide: Materials physics of orthorhombic In_2O_3," Phys. Rev. B **88**, 161201 (2013).

[66] K. D. Kundra and S. Z. Ali, "Thermal expansion of In_2O_3," J. Appl. Cryst. **3**, 543–545 (1970).

[67] Martin T. Dove, *Introduction to Lattice Dynamics* (Cambridge University Press, 1993).

[68] R. L. Weiher and R. P. Ley, "Thermal expansion of indium oxide," J. Appl. Phys. **34**, 1833–1834 (1963).

[69] Z. P. Yin, A. Kutepov, and G. Kotliar, "Correlation-enhanced electron-phonon coupling: Applications of *GW* and screened hybrid functional to bismuthates, chloronitrides, and other high-T_c superconductors," Phys. Rev. X **3**, 021011 (2013).

[70] Subhasish Mandal, R. E. Cohen, and K. Haule, "Strong pressure-dependent electron-phonon coupling in FeSe," Phys. Rev. B **89**, 220502 (2014).

[71] Matej Komelj and Henry Krakauer, "Electron-phonon coupling and exchange-correlation effects in superconducting H_3S under high pressure," Phys. Rev. B **92**, 205125 (2015).

[72] G. Antonius, S. Poncé, P. Boulanger, M. Côté, and X. Gonze, "Many-body effects on the zero-point renormalization of the band structure," Phys. Rev. Lett. **112**, 215501 (2014).

[73] Bartomeu Monserrat, "Correlation effects on electron-phonon coupling in semiconductors: Many-body theory along thermal lines," Phys. Rev. B **93**, 100301 (2016).